COBEM 2021 26th International Congress of Mechanical Engineering
November 22-26, 2021, Virtual Congress, Brazil

# COB-2021-1565
# EXPERIMENTAL DRAG REDUCTION ON AHMED BODY BY USAGE OF THE TRIP WIRES AND BY ARRANGEMENTS WITH MICROSPHERE

**Frederico Augusto Braga da Silva**
**Vagner Ferreira de Oliveira**
**Guilherme Papini**
**Rudolf Huebner**
**Rafael Miranda Hazaña Carvalho**
**Sarah Rodi Thomaz**
**Luiz Gustavo Miconi Soltz**
**Matthias Novais Keusen Reher**
**Thiago Aguiar Martins de Oliveira**
Universidade Federal de Minas Gerais UFMG – Av. Antônio Carlos, 6627, Campus da Pampulha - CEP 31270-901 - Belo Horizonte - MG
fred_emb@yahoo.com, vagnerunifei@gmail.com, papini@demec.ufmg.br, rudolf@demec.ufmg.br, rhazana@hotmail.com, srt@ufmg.br, luizsoltz@ufmg.br, matthias.nkr@gmail.com, aguiar20bh@gmail.com

***Abstract.*** *This article presents the studies carried out in the wind tunnel at the Federal University of Minas Gerais in order to verify the effects of the spheres arrangements and trip wires arrangements contributions on the total drag reduction of one proof test Ahmed's Body. To do this, sets of trip wires were placed at the Ahmed's Body, over its top surface and over its left and right sides. The spacing between each sphere and each trip wire, and their arrangements, were chosen in order to verify their effects and contribution on drag reduction. A baseline configuration without any devices was established to serve as reference. The best drag reduction result obtained from the experiments was 4% with spaced trip wire relative to baseline. The drag reduction mechanism due to spheres and wires arrangements is resulted from small disturbances on flow with a sequence of small detachments and reattachments of the boundary layer. The global effect is the delaying of the flow main separation, reducing the static pressure difference between the front and rear faces of the Ahmed's Body, leading to a pressure drag reduction. This mechanism was verified by means of CFD simulations. The friction drag increase due to the spheres and trip wires was evaluated at CFD simulations since it was not measured at experiment. It was verified to be negligible when compared with the total drag reduction obtained with the spheres and trip wires arrangements. In addition, CFD studies were performed in order to validate the Ahmed's Body simulation model, by the use of the wind tunnel results. The CFD simulations shown good adherence with the experiment, since the drag reduction obtained with simulation was 3.6 %. The validation of the current CFD analyses has demonstrated the utility of this tool to support future wind tunnel tests. The CFD simulations will allow the evaluation of a significant variety of configurations before wind tunnel test runs, saving cost and time expended with prolonged tests with this Ahmed's Body. The data collected from this study has potential application in the automobile, aeronautical, naval, and train transports industries, with positive impacts on economic and environmental parameters.*

***Keywords:*** *Aerodynamics, Ahmed Body, Automobile, Wind Tunnel, Drag Reduction, Trip Wires*

## 1. INTRODUCTION

The development of devices to reduce pressure drag in bluff bodies is, currently, a widely studied topic. These devices usually act through the manipulation of the turbulent flow in the wake of the bluff body and may consist of simple changes in the geometry of the body (passive control), actuators such as blowing air jets (active control), or a combination of both. The present paper aims to assess the efficiency of a geometry modification created by the addition of micro-spheres and trip wires in the Ahmed's Body, above the superior wall and at lateral sides. Both are passive control devices. The experiments were performed:

1. With the Ahmed's Body without modifications to set a reference;
2. With addition of two sets of micro-spheres;
3. With addition of two sets of trip wires on top of the superior wall and in each lateral side.

In the second and third conditions as described above, the placement and arrangement of the micro-spheres and trip wires were varied. The micro-spheres, in this application, are named vortex generators. Many variations of this type of device have been tested and experimented over the years. Gustavsson et al. (2006) summarizes several results for already tested technologies, including some variations of vortex generators. Previous studies have shown that placing a trip wires around sphere delays the separation of the boundary layer, reducing the overall drag of the sphere, Son et al. (2011), Oliveira et al. (2019). These results lead to a hypothesis that the trip wires may present a similar behavioral change in the turbulent flow when placed on a bluff body. Modifications somewhat similar to the micro-spheres addition, with the same application, have been performed by Viswanathan et al. (2021) and returned satisfactory results of up to 8.5% pressure drag reduction - small cylinders, named cylindrical vortex generators, were added in the rear, on top of the superior wall. Faruq et al. (2017) performs a modification by adding dimples on the superior wall of the Ahmed's Body, which possibly disturbs the flow similarly as the addition of trip wires, and achieves a drag reduction of approximately 6%.

## 2. TEST SETUP AND DATA COLLECTION

The tests were carried out at the facilities of the Aerodynamics Laboratory of the Federal University of Minas Gerais, in its Göttingen type closed-circuit wind tunnel. Figure 1 presents an isometric view of wind tunnel at UFMG. The air speed inside the wind tunnel was set for 30 m/s, 40 m/s, 50 m/s and 60 m/s when performing Ahmed's Body under clean configuration (baseline). The objective was to verify how the Reynolds number variation affects the drag coefficient. The range of Reynolds at test was between 2.00E+5 up to 4.00E+5. For the microspheres and trip wire tested configurations, the airspeed of 30 m/s was selected in order to diminish the detachment risk of the added geometries over the body. Also, the selection of 30m/s for the airspeed test was a good condition since it reproduces a typical ground vehicle cruise speed, that is approximately 110 km/hr. Equivalent approach was followed by Faruq et al. (2017). The average tested Reynolds number was 1.99E+5 for an average air temperature of 24 °C. Despite the wind tunnel facilities capability to allow setting the airspeed from 20 m/s up to 120 m/s, tests above the 60 m/s were not verified in order to minimize the risk of the damage on the Ahmed's Body due its fragile parts.

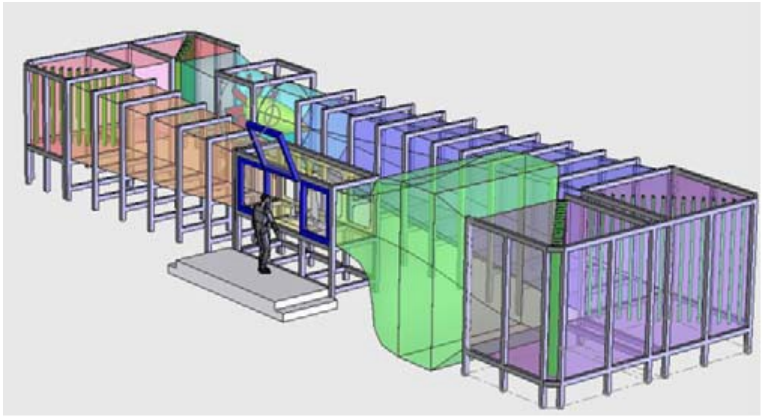

Figure 1 UFMG Wind Tunnel Facilities

Eight different geometry modifications were tested and are illustrated in Figure 2 and Figure 3. The placement of the modifications along the Ahmed's Body was also varied. A full description of all configurations tested and the placements tested for each configuration is indicated in Figure 4.

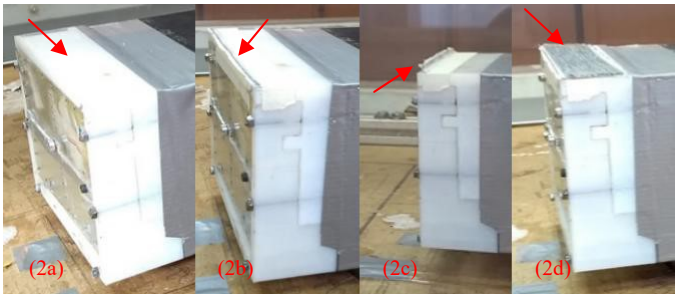


Figure 2 a) Clear (baseline); b) One wire attached; c) One wire unattached (free-floating); d) Multiple wires clustered

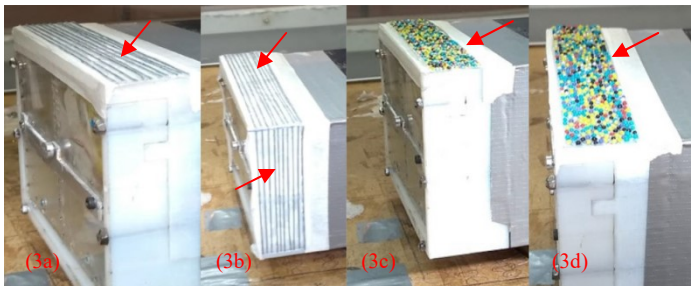


Figure 3 a) Multiple wires spaced - upper wall; b) Multiple wires spaced - upper and lateral walls c) Multiple microspheres clustered; d) Multiple microspheres spaced

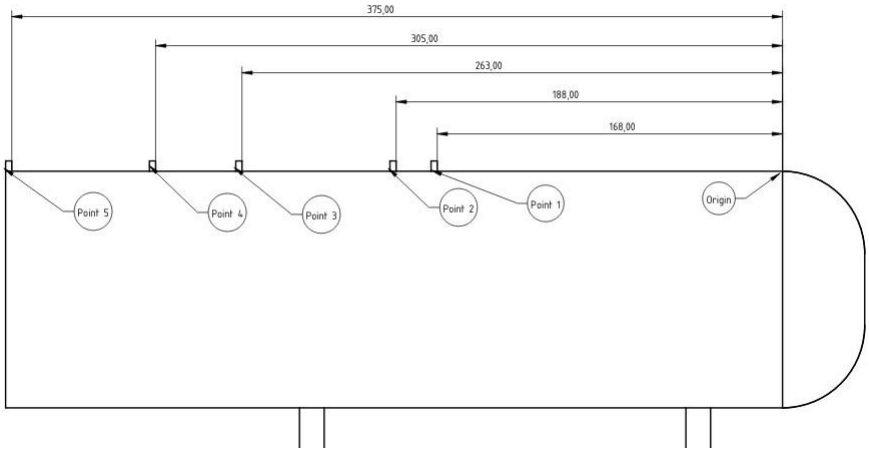


Figure 4 Indication of the placements tested (in mm)

For most of the configurations, the tests were repeated in order to provide a statistical base and to assure the collection of the correct behavior of the tested configuration. The Table 1 presents the numbers of runs of each tested configuration.

| **Geometry Modifier** | **Placement of the Disturbing Device *** | |
|---|---|---|
| - | Distance | Runs |
| Clear - baseline | - | 6 |
| One wire attached | 188 mm | 2 |
| | 375 mm | 5 |
| One wire unattached | 375 mm | 5 |
| Multiple wires clustered | 188 mm | 2 |
| | 375 mm | 5 |
| Multiple wires spaced - upper wall | 168 mm | 1 |
| | 188 mm | 2 |
| | 263 mm | 3 |
| | 375 mm | 5 |
| Multiple wires spaced - upper and lateral walls | 263 mm | 3 |
| | 375 mm | 5 |
| Multiple microspheres clustered | 188 mm | 2 |
| | 375 mm | 5 |
| Multiple microspheres spaced | 188 mm | 2 |
| | 263 mm | 3 |
| | 305 mm | 4 |
| | 375 mm | 5 |

*Measures taken from the origin point indicated in Figure 4

Table 1 - Tested configurations and respective placements

The diameter of the microspheres and of the trip wires were chosen based on the theoretical boundary layer thickness over the Ahmed's Body under 30 m/s, atmosphere of 1 atm and air temperature of 20 °C. The theoretical boundary layer thickness was calculated using the Equation 1. The estimated boundary layer thickness was 0.81 mm. The ideal condition should be reached when the microspheres and trip wires are all immersed within the boundary layer thickness.

$$\frac{\delta^*}{x} = \frac{1.7208}{\sqrt{R_e}} \quad (1)$$

Table 2 and Figure 5 provide more details about the array of the microspheres and trip wires sets. Each set of disturbing devices was fixed at Ahmed's Body with speed tape.

| | |
|---|---|
| Mean diameter of the microspheres ($D_e$) | 1.5 mm |
| Mean diameter of the wires ($D_a$) | 1 mm |
| Clustered microspheres | 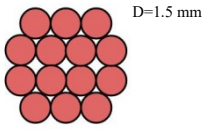  |
| Spaced microspheres | 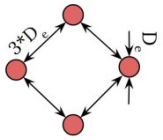  |
| Clustered wires |  |
| Spaced wires |   |

Table 2 - Details of the test layout

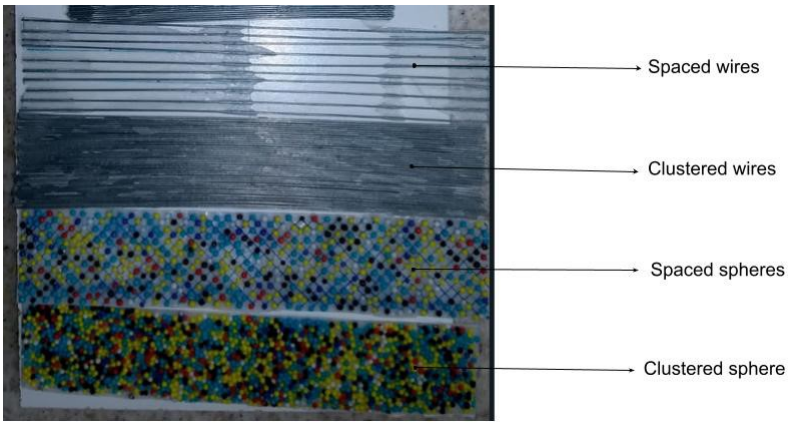


Figure 5 Modifiers added in the Ahmed's Body

The data collection was initiated as soon as the air flow in the wind tunnel was stabilized. This was reached 5 minutes after the test run start.

The relevant wind tunnel data were collected by appropriate systems and transducers:

- Voltage acquisition system through an instrumented load cell (volts);
- Air flow mass temperature: static air temperature sensor (°C);
- Static air pressure and total flow pressure: pressure transducers;
- Dynamic pressure: pressure transducer (Pa);

## 3. RESULTS

The data acquired were reduced in order to put all results at the same reference bases. According to the data reduction analyses, all sets of wires and microspheres experienced some drag effect when implemented over the Ahmed's Body relative to the baseline configuration. There were cases where the disturbing device set increased the drag relative to the baseline configuration and cases that a drag reduction was observed relatively the baseline configuration. For the cases where a drag reduction was noticed, the drag reduction mechanism due to spheres and wires arrangements is resulted from small disturbances on flow with a sequence of small detachments and reattachments of the boundary layer at top of the Ahmed's Body. As can be verified on the graph below, the set of spaced wires presented better results when compared with all other sets of wires and microspheres. A notable result was

achieved when a set of spaced wires were positioned at the top at 188 mm from the front face of the tested Ahmed's Body. The Figure 6 presents the drag reduction in percentage of each tested configuration comparatively with the baseline.

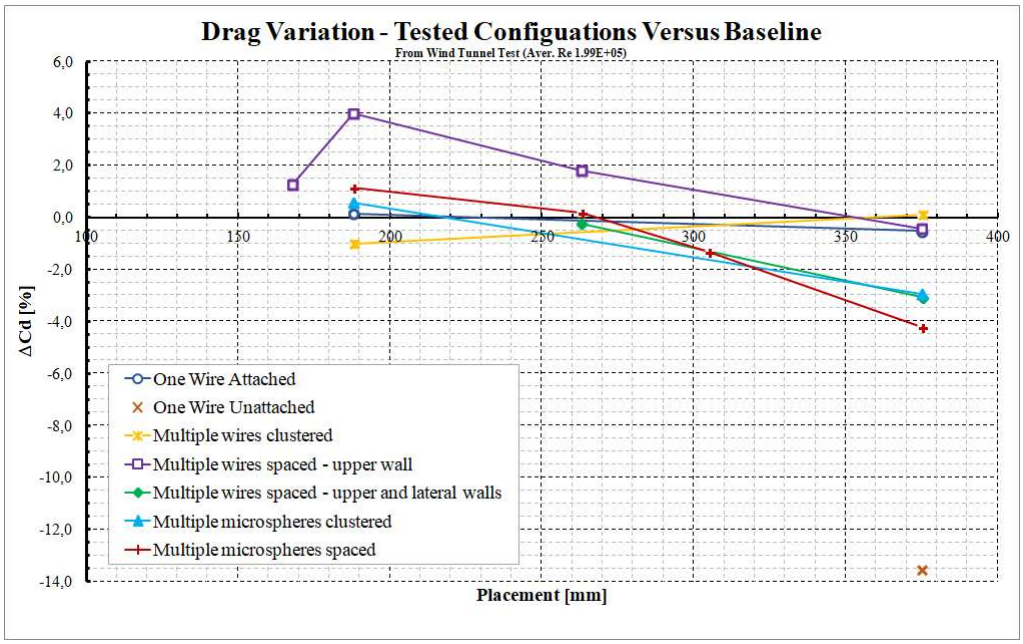


Figure 6 Drag reductions from the tested configurations

The data that composed the Figure 6 are presented in Table 3.

| Baseline Drag (Clear Ahmed Body) | Cd | | | | | | |
|---|---|---|---|---|---|---|---|
| | - | | | | | | |
| | 0,4590 | | | | | | |
| Tested Configuration | Position | Running Nº | Air Temperature | Air Speed | Re | Cd | −Cd |
| - | mm | - | °C | m/s | | - | % |
| One wire attached | 188 | 2 | 29,4 | 30,1 | 1,98E+05 | 0,4583 | 0,1 |
| | 375 | 5 | 28,9 | 30,1 | 1,98E+05 | 0,4614 | -0,5 |
| One wire unattached | 375 | 5 | 29,3 | 30,1 | 1,98E+05 | 0,5211 | -13,5 |
| Multiple wires clustered | 188 | 2 | 29,2 | 30,1 | 1,98E+05 | 0,4637 | -1,0 |
| | 375 | 5 | 29,2 | 30,1 | 1,98E+05 | 0,4585 | 0,1 |
| Multiple wires spaced - upper wall | 168 | 1 | 29,6 | 30,1 | 1,98E+05 | 0,4532 | 1,3 |
| | 188 | 2 | 29,6 | 30,1 | 1,98E+05 | 0,4407 | 4,0 |
| | 263 | 3 | 26,3 | 30,1 | 2,02E+05 | 0,4507 | 1,8 |
| | 375 | 5 | 25,8 | 30,2 | 2,02E+05 | 0,4609 | -0,4 |
| Multiple wires spaced - upper and lateral walls | 263 | 3 | 26,8 | 30,1 | 2,02E+05 | 0,4601 | -0,2 |
| | 375 | 5 | 27,0 | 30,1 | 2,02E+05 | 0,4731 | -3,1 |
| Multiple microspheres clustered | 188 | 2 | 29,6 | 30,0 | 1,98E+05 | 0,4564 | 0,6 |
| | 375 | 5 | 29,6 | 30,0 | 1,97E+05 | 0,4725 | -2,9 |
| Multiple microspheres spaced | 188 | 2 | 29,3 | 30,1 | 1,98E+05 | 0,4538 | 1,1 |
| | 263 | 3 | 28,6 | 30,1 | 1,99E+05 | 0,4582 | 0,2 |
| | 305 | 4 | 29,0 | 30,1 | 1,99E+05 | 0,4651 | -1,3 |
| | 375 | 5 | 27,8 | 30,2 | 1,99E+05 | 0,4784 | -4,2 |

Table 3 – Data reduction Summary

The baseline configuration was evaluated over six runs. Three runs in 30 m/s, and for 40 m/s, 50 m/s and 60 m/s, with one run. The purpose of airspeed variation was to identify how the drag coefficient behaves under Reynolds

variation. Figure 7 presents the Cd over Reynolds variation. A light drag reduction tendency can be noticed as the Reynolds increases. Similar behavior was noticed in the experiment carried out by Oliveira et al. (2019). This phenomenon is called 'drag crisis' and the Reynolds number at which the drag coefficient becomes minimum is called critical Reynolds number.

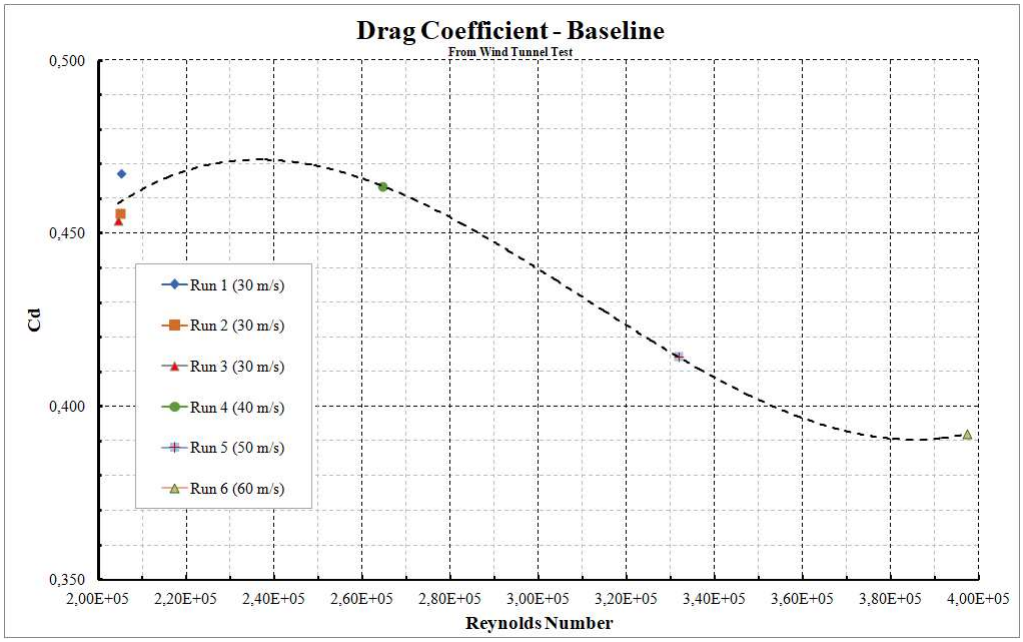


Figure 7 Drag Coefficient Versus Reynolds

The data derived from the airspeed of 30 m/s were used for the baseline drag determination, since all disturbing devices tested were performed in this condition. The average baseline drag coefficient obtained was 0.4590. Table 4 presents the baseline drag results.

| Tested Configuration | Running Nº | Air Temperature | Air Speed | Re | Cd |
|---|---|---|---|---|---|
| - | - | °C | m/s | - | - |
| Baseline | 1 | 23,3 | 30,1 | 2,05E+05 | 0,4674 |
| | 2 | 23,7 | 30,1 | 2,05E+05 | 0,4557 |
| | 3 | 24,0 | 30,1 | 2,05E+05 | 0,4538 |
| | 4 | 29,3 | 40,2 | 2,65E+05 | 0,4635 |
| | 5 | 29,9 | 50,4 | 3,32E+05 | 0,4144 |
| | 6 | 29,5 | 60,3 | 3,97E+05 | 0,3921 |

Table 4 – Baseline Drag Coefficient

The standard deviation for the drag force was 0.29 N. The uncertainty was 0.09 N. The sample length with 99 % of certainty required for the experiment was 56 samples. Considering that all data was recorded at a sample rate of 200 samples/second, the time window of 1 minute for data collection proved to be enough to get the confidence required for the test.

Next paragraph presents the data collection and data reduction methodologies adopted.

## 4. DATA REDUCTION METHODOLOGY

The data reduction methodology consisted essentially in the determination of the drag coefficient of each tested configuration. The equations used for data reduction are presented below.

The data sample used for data reduction was obtained from data recorded at each run. The data sample was corresponding to the data available in the last 60 seconds recorded. From this sample, the calculation of each parameter was done in the same sample rate. The following parameters were calculated:

- Drag force:

$$F = \frac{(Volts_{Load\ Cell} - 1)}{4} * 5 * 9.81\ (N) \quad (2)$$

a) N: Newton;
b) 5: factor to convert volts in gram force;

- Drag coefficient:

$$C_D = \frac{F}{(C_{H0} * S_{AB})} \quad (3)$$

c) Reference Ahmed's Body area: $S_{AB} = 0.018305$ m$^2$;
d) Dynamic pressure from pressure transducer, channel 1 $C_{H0}$ (Pa);

- Reynolds number:

$$R_e = \frac{\rho}{\mu} UL \quad (4)$$

e) Airspeed in wind tunnel section: $U\ (m/s)$;
f) Characteristic length: $L = 0.378\ (m)$;
g) $\rho$: air density (kg/m$^3$);
h) $\mu$: Dynamic viscous (kg/ms);

- Air density:

$$\rho = \frac{2C_{H0}}{V^2} \left(\frac{kg}{m^3}\right) \quad (5)$$

- Dynamic viscosity:

$$\frac{\mu}{1.71E-5} \approx \left(\frac{T}{273.15}\right)^{\frac{3}{2}} \left(\frac{383.55}{T + 110.4}\right) \left(\frac{kg}{ms}\right) \quad (6)$$

i) Air temperature: $T\ (K)$;

- Delta drag coefficient:

$$\Delta C_D = \frac{C_{DBase\ Line} - C_D}{C_{DBase\ Line}} * 100\ (\%) \quad (7)$$

- Standard deviation:

$$\sigma = \sqrt{\frac{\sum_{i=1}^{n} (F_i - F_{Aver})^2}{n}} \quad (8)$$

j) $F_{Aver}$: Sample average force (N);
k) n: Sample length;

- Sample length:

$$n = \left(\frac{2.57 * \sigma}{error}\right)^2 \quad (9)$$

l) error: Load cell error = $\pm 0.02\%$;

- Uncertain:

$$uncert = F_{Aver} \pm 2.57 * \frac{\sigma}{\sqrt{n}} \quad (10)$$

## 5. SIMULATIONS

To verify and further expand the understanding of the phenomena, there were simulations made to contrast with the experimental data. The best scenario and the baseline were chosen to create a valid comparison and to further enhance our understanding of the phenomena studied. The model created was made following the dimensions of Table 2 and the following Figure 8.

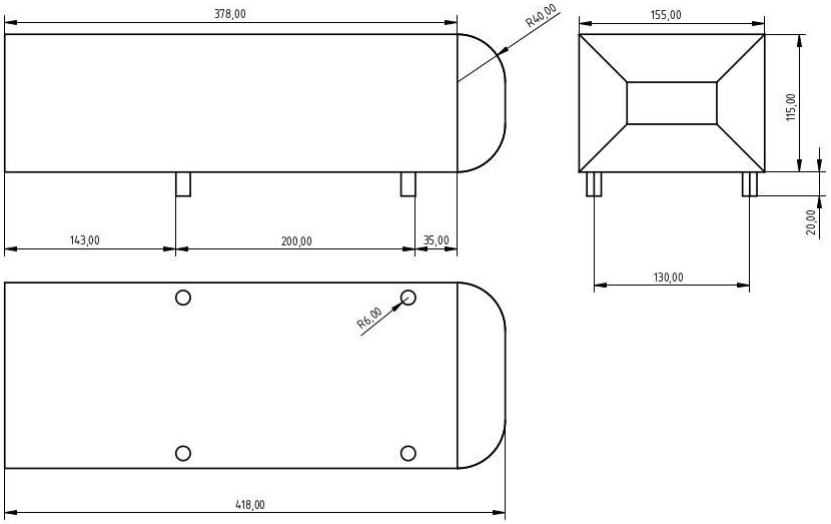


Figure 8 3D Model Used in the Simulations (Units in mm)

To create a mesh over the model there was made a control volume with the same dimensions of the wind tunnel test section, and by placing the Ahmed's Body in the same position as tested the setup for meshing was complete. The method of meshing chosen was to use hexahedral elements on the entire domain and a set of prisms extruding from the surface of the Ahmed's Body, so there was a way to properly capture the boundary layer viscous behaviors. This inflation layers meshing approach is essential for capturing the viscous effects of near-wall flow. The reference used for the wall sizing was a y+ based approach, on which the entire surface of interest would be covered by elements with spacing with y+ equal or less than 1. The general fluid domain was set to have a maximum element size of no more than 500 times the wall spacing to ensure a good behavior of the solver and there were many local refinements over the main flow transition volumes of the Ahmed's Body in order to ensure no phenomena would be missed. The mesh results for both simulations were:

| Simulated Condition | Nº of Mesh Elements | Element Maximum Skewness |
|---|---|---|
| Baseline | 1419111 elements | 7.7 deg |
| Trip wires @188mm | 6057122 elements | 8.4 deg |

Table 5 – Mesh Characteristics

The solver used was the SST k-ω and in contrast to Faruq et al. (2017) that used Spalart-Allmaras. It is understood that the phenomenon of interest is entirely dependent on the viscous part of the flow. Therefore, by using a model that linearizes this behavior, there would be a significant loss of data, and this is noticed clearly by the values of the experimental and simulated conditions of this paper being significantly lower than those predicted. By choosing a RANS approach it is clear that the numerical data and experimental data will be more entwined given the nature of the collection methodology, being over a long period of time as if an averaged value. The choice of k-ω instead of its brother k-ε was due to its more elaborate treatment of the diffusivity term, which for the experiment is fundamental in understanding the flow. Modeling the wake region and boundary layer transition point are key aspects for the experiment physics. Since these phenomena are directly linked to the viscous effects of the flow, the k-ω approach is more adequate, due to its better approach on near-wall viscous effects. At least it was used the Menter approach to shear

stress transition (SST) for its better evaluation of the flow transition without an extreme computational cost added, since the blending function transition between k-ε model, which is a faster model in computational aspect, on the freestream flow, and the k-ω model in near-wall regions, where the viscous forces are relevant and must have a more refined approach. Those choices achieved a good relation between computational accuracy and cost, giving good numerical results and consistent data for comparison with the experiments made.

The results of the simulation gave a result of 3.6% drag reduction for the best configuration, and therefore it is remarkably close to the experimental data of 4%, and therefore can be used to better understand the flow patterns and behavior over the Ahmed body. The convergence of the simulation was defined using continuity of the flow patterns at 1E-5 and a stabilization of the reference value of interest, the drag coefficient. Given that there is an unsteady flow and the use of RANS on a steady configuration, there is bound to have oscillations due to the coupling of pressure and velocity fields and for that the floating average of the drag coefficient was taken instead of a single data point. By doing this it is further increased the validity of the computational processes as the data collection in both the experiment and numerical fields are taken in a similar fashion of averaged values from an unsteady flow.

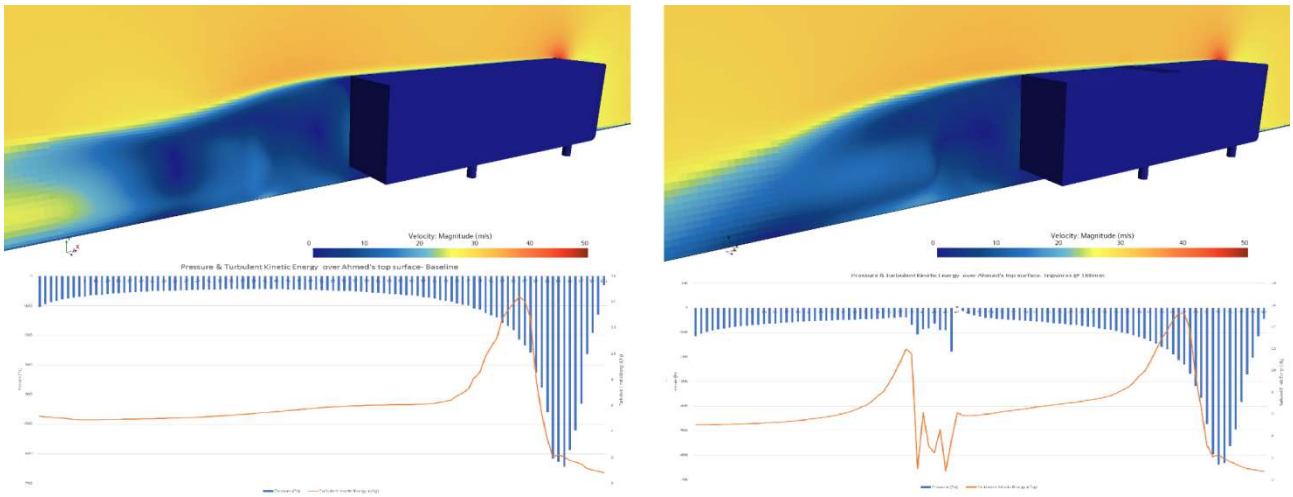


Figure 9 Side by Side Comparisons of Velocity Fields, Pressure and Turbulent Kinetic Energy

In Figure 9 the left image is the reference and the other one is the configuration with the best results, tripwires at 188mm from the front. It is notable the difference on the recirculation bubble at the back of the body and the much more behaved flow on the second image, leading to a smaller low pressure zone that reduces pressure drag. It is noticeable that friction drag is next to irrelevant as the perturbations only cause a small re-energization of the boundary flow. It can also be noticed the effect the tripwires have on the pressure distribution atop the Ahmed's Body and the correlation with a spike in turbulent kinetic energy, showcasing the mechanism of drag reduction via energization of the flow.

## 6. CONCLUSIONS

The Ahmed's Body is a simplified vehicle model that can represent generic car, bus, train and many other terrain vehicles on aerodynamic studies at wind tunnels and in CFD analysis. The benefits of the trip wires were verified when correctly positioned on a sphere and on an Ahmed's Body producing significant drag reduction, Son et al. (2011), Oliveira et al. (2019). By analogy with the dimple effect, Faruq et al. (2017), the spaced trip wires arrangements produced small disturbances on flow with a sequence of small detachments and reattachments, increasing the turbulent boundary layer momentum at the rear of the Ahmed's Body. This phenomenon was captured by the CFD simulations. The spaced trip wires over the Ahmed's Body produced drag reductions when compared with the baseline. Notable drag decrease, 4%, was observed when spaced wires were positioned at top of Ahmed's Body at 188 mm from the front face. In addition, the CFD simulation has shown consistent adherence with the wind tunnel results, since the drag decrease of 3.6% was achieved under same conditions of the experiment. This CFD model can be used as a powerful tool for future studies, allowing the understanding of the aerodynamic characteristics before the tests in the wind tunnel with this Ahmed's Body.

## 7. REFERENCES

Ahmed, S. R.; Ramm, G.; Faltin, G. 1984. "Some Salient Features of the Time-Averaged Ground Vehicle Wake." *SAE*

*The Engineering resource for advancing mobility* (February 27-March 2): 31.

Chadwick, Andrew, Kevin Garry, and Jeff Howell. 2010. "Of Simple Vehicle Shapes by the Measurement of Surface Pressures Reprinted From : Vehicle Aerodynamics." *Society* (724).

Faruq, A.L.M., M.N.M. Zain and Azwar, A.M., 2017. "The Introductory of Dimple to the Ahmed Body Top Surface as a Drag Reduction Device, Proceedings of Mechanical Engineering Research Day 2017, pp. 64-65, Mei 2017.

Fluent, ANSYS. 2011. "Ansys Fluent Theory Guide." *ANSYS Inc., USA* 15317(August): 724–46.

Guilmineau, Emmanuel, and Francis Chometon. 2010. "Numerical and Experimental Analysis of Unsteady Separated Flow behind an Oscillating Car Model." *SAE International Journal of Passenger Cars - Mechanical Systems* 1(1): 646–57.

Hucho, I., Wolf-Heinrich Hucho, Gino Sovran, and I. Hucho. 1993. "Aerodynamics of Road Vehicles." *Annual Review of Fluid Mechanics* 25(1): 485–537. http://fluid.annualreviews.org/cgi/doi/10.1146/annurev.fluid.25.1.485.

Krajnović, Siniša, and Lars Davidson. 2005. "Flow Around a Simplified Car, Part 2: Understanding the Flow." *Journal of Fluids Engineering* 127(5): 919.

Malalasekera, H K Versteeg and W. 2007. *An Introduction to Computational Fluid Dynamics THE FINITE VOLUME METHOD*. Second edi. Pearson Education Limited.

McCallen, Rose, Richard Couch, and Juliana Hsu. 1999. "Progress in Reducing Aerodynamic Drag for Higher Efficiency of Heavy Duty Trucks (Class 7-8)." *SAE Technical Paper Series* 1(1999-01–2238): 9.

Metz, Norbert. 2001. "Contribution of Passenger Cars and Trucks to CO2, CH4, N2O, CFC and HFC Emissions." *SAE TECHNICAL PAPER SERIES* (724).

Minguez, M., R. Pasquetti, and E. Serre. 2008. "High-Order Large-Eddy Simulation of Flow over the 'Ahmed Body' Car Model." *Physics of Fluids* 20(9).

Oliveira, V. F., Huebner, R. and Roque, G., 2019. "COB-2019-0811 "Optimization of Drag Reduction by a Different Trip Wires Diameters Variation on a Sphere".

Son, K., Choi, J., Jeon, W.P. and Choi, H., 2011. "Mechanism of Drag Reduction by a Surface Trip Wire on a Sphere". Journal of Fluid Mechanics, Vol. 672, pp. 411–427. ISSN 14697645. doi:10.1017/S0022112010006099.

## 8. RESPONSIBILITY NOTICE

The author(s) is (are) the only responsible for the printed material included in this paper.